High-throughput microCT scanning of small specimens: preparation, packing, parameters and post-processing

Christy A. Hipsley[1,2*], Rocio Aguilar[1,2,3], Jay R. Black[4], Scott A. Hocknull[1,5]

[1]School of BioSciences, University of Melbourne, Parkville, VIC, 3010, Australia.

[2]Museums Victoria, GPO Box 666, Melbourne, VIC, 3001, Australia.

[3]School of Biological Sciences, Monash University, Clayton, Victoria, Australia.

[4] School of Earth Sciences, University of Melbourne, Melbourne, Victoria, Australia.

[5]Queensland Museum, Geosciences, 122 Gerler Rd. Hendra, Queensland, 4011, Australia.

*Corresponding author:

Christy A. Hipsley

University of Melbourne

BioSciences 4, Building 147

Parkville, VIC 3010

Australia

christy.hipsley@unimelb.edu.au

Running title: High throughput microCT scanning of small specimens

Abstract

High-resolution X-ray microcomputed tomography, or microCT (μCT), enables the digital imaging of whole objects in three dimensions. The power of μCT to visualise internal features without disarticulation makes it particularly valuable for the study of museum collections, which house millions of physical specimens documenting the spatio-temporal patterns of life. Despite its potential for comparative analyses, most μCT studies include limited numbers of museum specimens, due to the challenges of digitising numerous individuals within a project scope. Here we describe a method for high-throughput μCT scanning of hundreds of small (< 2 cm) specimens in a single container, followed by individual labelling and archival storage. We also explore the effects of various packing materials and multiple specimens per capsule to minimize sample movement that can degrade image quality, and hence μCT investment. We demonstrate this protocol on vertebrate fossils from Queensland Museum, Australia, as part of an effort to track community responses to climate change over evolutionary time. This system can be easily modified for other types of wet and dry material amenable to X-ray attenuation, including geological, botanical and zoological samples, providing greater access to large-scale phenotypic data and adding value to global collections.

Keywords

X-ray microcomputed tomography, microCT, CT scan, 3D imaging, fossils, geometric morphometrics, high-throughput

Introduction

High-resolution X-ray microcomputed tomography, also known as HRXMT or microCT (μCT), is an increasingly powerful tool for the non-destructive investigation of whole objects. Functioning like a microscope with X-ray vision, μCT generates high fidelity 3D models of solid material from which the outer layers can be virtually dissected or removed, revealing the inner structure. Starting with radiographs of an object taken over multiple angles, a computer algorithm is used to digitally reconstruct a stack of 2D X-ray projections, or tomograms, into a 3D volume. Whereas in human medicine the X-ray source rotates around the patient (e.g., computerized axial tomography, or CAT scan), in μCT the object is typically fixed on a rotating stage while the X-ray tube remains stationary. The differential properties of the object's matter, including thickness and atomic number, interact with the X-ray's energy beam to determine the number of photons that pass through it to reach the detector on the other side. This decrease in electromagnetic radiation, termed X-ray attenuation, results in detector pixels with grayscale values proportional to the radiopacity of the material, meaning that dense regions such as bone or rock appear white or light gray (radiopaque), while muscle or skin appears dark (radiolucent). The improved resolution of μCT over standard imaging techniques can achieve a detail detectability down to 200 nm (0.2 micrometre) – less than the diameter of a single red blood cell.

Since publication of the first X-ray microtomographic figures nearly four decades ago[1,2,3], μCT has had profound impacts across scientific disciplines. Studies in biomedicine, zoology, geology and paleontology now regularly incorporate μCT images[4,5,6], and open source software for the quantitative analysis of volumetric data is developing rapidly (e.g., Fiji[7], Blob3D[8], Dragonfly [Object Research Systems (ORS) Inc., Montreal, Canada]). Within the biological sciences, μCT has been particularly valuable for the study of museum collections, which contain millions of often small, delicate and unique specimens not

69 amenable to traditional (destructive and/or irreversible) preparation. Worldwide, these
70 collections span taxonomic, geographic and temporal distributions, providing a wealth of
71 information for understanding the past, present and future of biodiversity[9]. Creation of
72 cybertypes, or virtual models of type material, is another emerging application of μCT
73 technology[10,11], allowing researchers around the world to interact with voucher specimens.
74 When combined with downstream analyses like geometric morphometrics, these models can
75 be used to test taxonomic hypotheses that could shorten the lagtime between species
76 discovery and formal description[10,12], thus expanding the taxonomic bottleneck.

77 Despite the increasing use of μCT in systematic biology[13], a major challenge remains
78 in the practical imaging of high numbers of museum specimens within a project scope, for
79 example in the context of large-scale analyses of phenotypic variation. This has proven
80 difficult because of the need for samples to remain motionless during scan time (minutes to
81 hours), and because each individual must be digitally labelled to match the physical
82 specimen's identity and hence retain important information, e.g., material type, locality,
83 stratigraphic age. These issues have so far limited community-level μCT analyses, which
84 could provide important insights into evolutionary responses to environmental change in
85 small, rare, and/or fossilized taxa[6]. While other mass digitisation efforts of museum
86 collections are already under way, they are typically limited to high resolution photographs of
87 entire drawers to capture external morphology[14,15]. However internal structures are among the
88 fastest responders to environmental drivers, suggesting an untapped role for μCT data in
89 climate change research[6]. Especially in the Anthropocene, μCT offers a promising digital
90 technique to identify the evolutionary consequences of human activities in natural history
91 collections at both the internal organismal and ecosystem levels[16,17].

92 Although some digital morphology studies have included hundreds of[18,19] or over a
93 thousand[20,21,22,23] 3D models, their images are often aggregated using different sources

94 (museums, repositories, laboratories), methods (surface scanning, μCT), and parameters (X-
95 ray energy, voxel size, number of projections), making it difficult to integrate and compare
96 findings. For smaller specimens in particular, variation in spatial resolution can result in
97 significant measurement errors, for example in estimated volumes or relationships between
98 traits[24,25]. Limitations on time and money for μCT scanning also mean that specimen data are
99 often collected haphazardly, constraining systematic analyses to one or few individuals per
100 species[6]. This trade-off between data accessibility and data quantity (and quality[26]) precludes
101 the opportunity for more rigorous investigations of phenotypic diversity in time and space, as
102 well as focused analyses of variation in a single taxon or locality. Common biodiversity
103 metrics such as species identity, richness, and evenness are inferable from μCT data, e.g.,
104 [27,28], especially for cryptic taxa and species complexes with few observable differences[29,23,31].
105 Therefore, optimisation of the scanning process for high resolution 3D images of multiple
106 specimens would not only contribute to our understanding of how biodiversity responds to
107 global change, but also to the value of museum collections and researchers' abilities to access
108 them.

109 Here we outline steps for the high-throughput μCT scanning of small (< 2 cm) fossils,
110 meant to facilitate advanced exploration of museum collections and allow researchers with
111 limited access to specialized facilities the opportunity to maximize their investments. In
112 contrast to other high-throughput μCT methods that have focused on clinical evaluations[32,33]
113 or automated phenotyping of laboratory strains (e.g., mice[34], rice[35], zebrafish[36]), we
114 concentrate on the practical arrangement of accessioned museum specimens so that each
115 individual can be identified and labelled in the 3D volume, followed by long-term storage
116 and archiving. We illustrate this method using vertebrate (reptile, amphibian and mammal)
117 fossils from the paleontological collections of Queensland Museum, Australia, as part of a
118 larger effort to identify changes in morphology and species assemblages over geological

time. We succeed in maximizing the quantity of fossils per container to over 200 specimens to generate high quality 3D models for comparative analyses, while minimising associated time, handling, and error. These steps should be applicable to any small dry objects amendable to X-ray attenuation including geological material, plant tissues, and invertebrates, and wet specimens provided they can be mounted inside small capsules or other containers[37,38].

Methods

Preparation

The first step is the only time the user is required to handle specimen material directly, we therefore recommend the use of featherweight spring or feather light forceps and secondary containment (see Figure 1 for an overview of packing material). Although specimens of varying size can be scanned together, it is preferable to organise fossils into batches of roughly similar material properties for X-ray optimization. Thin, unbuffered, neutral pH tissue is ideal for specimen packing and eventual long-term storage. Other required materials are small clear two-piece pharmaceutical capsules, paper and/or plastic drinking straws, archival paper and pen for labelling, a 50 ml plastic centrifuge tube with cap, and medium density polyethylene foam. Suggested suppliers and estimated costs of material per tube are listed in Table 1.

Packing procedure

Briefly, each specimen is wrapped in archival tissue and placed inside a capsule with its label, several of which are inserted lengthwise into a straw. Up to 14 standard paper straws cut to 9 cm in length fit inside a closed 50 ml Falcon tube, with each straw holding 6 size 4 capsules. For easier tracking of specimens in the 3D volume, we recommend leaving one

144 capsule empty in different positions along the length of some straws (see post-processing
145 section below). Following this method, over 80 specimens < 1 cm long can be scanned in a
146 single tube. This quantity can be doubled or tripled when 2 or 3 fossils (separated by tissue)
147 are packed inside the same capsule, allowing a maximum of 252 specimens. However, scans
148 with more than 3 specimens per capsule showed a high (≥ 50%) rate of movement during
149 rotation, compared to those with fewer (Table 2). We therefore limit packing to 1-2
150 specimens per capsule, provided they can be distinguished from one another in relative size
151 and/or shape. Specimens up to 2 cm long can be similarly packed inside size 00 capsules.
152 Larger diameter paper or smoothie straws sliced lengthwise hold 3 size 00 capsules in a 50 ml
153 tube (Fig. 1b), which can be scanned together with smaller straws as needed.

154 Labels for each specimen are written in Indian or archival ink on uncoated acid-free
155 paper, providing a unique and durable identifier that will be matched in the 3D volume. Our
156 labels followed a two-part system containing specimen ID (e.g., museum accession number)
157 and a code for straw and capsule position. Using permanent marker, each straw is labelled
158 with a letter (A, B, C…N for 14 straws) and each capsule is labelled with its straw's letter
159 and a number from 1-6, denoting its position in the straw from top to bottom (Fig. 2a). This
160 system can be amended to suit user needs, for example by including abbreviations for taxon if
161 known and/or material (e.g., 'il' for ilium, 'max' for maxilla). These codes can also be
162 extracted from the digital labels and used as variables in downstream analyses, e.g., in the R
163 statistical package geomorph[39] or MorphoJ[40]. Record labels with capsule and straw positions,
164 including any empty capsules as a marker, since these will be checked off later during
165 unpacking.

166 Once labelling is complete, the specimens, labels, capsules and straws are aligned for
167 packing. Each specimen is wrapped in a small envelope of Green's Lens tissue (Fig. 2b), and
168 empty spaces in the capsule are filled with tissue so the specimen does not contact its walls.

169 This creates more distance between adjacent samples, allowing easier separation (i.e.
170 segmentation) in the 3D volume. The tissue also prevents movement during image
171 acquisition (Table 2), which can lead to motion artefacts in the reconstruction like shadows or
172 streaking. Finally, the label is inserted into the capsule with the ID facing out for long-term
173 storage, and the capsules are loaded into their respective straws in the correct order. A thinner
174 cocktail straw can be used to gently push the capsules down without compressing ones below
175 it (Fig. 2c).

176 To load the packed straws into the Falcon tube, first fill the conical tip with
177 polyethylene or other firm material to create a flat surface. Insert the straws with position 1
178 towards this end, which will be facing up in the μCT machine. The flat surface of the cap on
179 the other end can be fixed to a glass rod or dowel using a hot glue gun to elevate the tube
180 from the machine's stage (Fig. 2d). This avoids including the metal clamp in the scan which
181 could affect X-ray optimization, and centres the tube vertically and horizontally relative to
182 the detector. Draw a diagram of the straw arrangement with the list of specimen labels, noting
183 where paper or empty straws are used to separate them for easier identification (Fig. 2e,f).
184 This material will be visible in reconstructed cross-sections, allowing one to match the 3D
185 volume to the diagram. Finally, medium density foam can be cut and placed as filler around
186 the straws and under the cap of the tube before closing. This foam is recommended over
187 tissue or other supporting material as it acts as an effective shock absorber during rotation.
188 Secure the tube onto the stage, making sure it can rotate freely without touching the X-ray
189 source or detector.
190

191 **X-ray parameters**

192 Scan settings vary depending on the equipment, material size and properties, and desired
193 results. Here we report parameters as optimised on a Phoenix nanotom m (GE Sensing &

194 Inspection Technologies GmbH, Wunstorf, Germany) equipped with a 180 kV, 20 W high-
195 power nanofocus X-ray tube and DXR detector (3072 x 2400 pixels). As with all
196 microtomographic imaging, initial calibration of the detector is largely software-driven to
197 reduce potential noise due to defective pixels or incident light. We calibrated the detector by
198 taking an offset image (dark field) and two sets of gain images (flat field) at the same energy
199 of the scan and at half the current, where images were averaged over 100 snapshots of the
200 detector with a skip of 10. For all scans our instrument was fitted with a tungsten target,
201 although molybdenum may be preferable for amber[4]. Fossils can be radiodense, in such cases
202 reconstruction artefacts may occur when lower energy X-rays are attenuated at the surface, or
203 when stronger X-rays hit the detector without passing through the object first (beam
204 hardening)[4]. A thin metal filter placed in front of the X-ray source can overcome these issues
205 by removing lower energy photons, although other parameters like current, voltage, or
206 exposure time should be modified to achieve appropriate contrast.
207 Ideally the number of images for reconstruction is equal to the maximum width of the
208 scanned object in pixels × $\pi/2$[38,41]. For a sample optimized to fill the full width of our
209 detector, this would result in nearly 5,000 projections at a resolution of 10.6 µm. Such a data
210 set would be massive in terms of scan time and storage (up to 70 GB before reconstruction),
211 in addition to the computing power and time needed to reconstruct and render each of the 3D
212 files individually. To improve the µCT process for smaller specimens without sacrificing
213 image quality, we divided the Falcon tube into three segments by moving the position of the
214 stage up or down between scans, while keeping all other settings identical. This produced
215 separate volumes of equally high quality while avoiding the need to move the detector back
216 and/or the tube forward to accommodate its length, thereby decreasing resolution. These
217 volumes can be merged using Avizo (Thermo Fisher Scientific) or other dedicated software
218 to recreate the entire tube in high resolution. However, for faster processing we aligned each

219 segment to include two rows of size 4 capsules (or one row of size 00), so they could be
220 separately visualised and labelled in the 3D volume if preferred.
221 For all reconstructions we followed the standard protocol of the Phoenix datos|x
222 software (GE Sensing & Inspection Technologies GmbH, Wunstorf, Germany), which tests
223 for object movement by comparing the first and last 2D projections. At high resolution, even
224 minute movements can cause visible artefacts in the reconstructed images[4,38]. Instead of
225 correcting for movement of single specimens during reconstruction by shifting the axis of
226 rotation (which would in turn generate artefacts in the rest of the tube), we identified and
227 labelled those specimens in post-processing so they could be rescanned. Other settings
228 applied during reconstruction were a 3×3 median filter and an ROI filter.
229
230 **Computed tomography post-processing**
231 Following reconstruction, digital labelling of the specimens is performed in 3D volume
232 rendering software. Here we describe steps using VGStudioMax 3.1 (Volume Graphics,
233 Heidelberg, Germany), although other options for free or commercial licenses are available
234 (see Table 7 in Keklikoglou et al.[38]). To match the tube orientation to the diagram (Fig. 2f),
235 the volume can be rotated in the 3D window or by using the registration tool in 2D. Straws
236 can then be labelled digitally with the indicator tool or by creating a region of interest (ROI)
237 to name each one by its letter (A, B, C… N). Similar-sized capsules should be aligned across
238 the straws horizontally, making it easy to identify capsule positions in the 2D and 3D
239 windows. For example, starting from the top (tip) of the tube in straw A, specimens should be
240 ordered as A1, A2…A6, with capsules in the neighbouring straw B following the same order.
241 Verifying the positions of empty capsules is another safeguard to ensure correct orientation.
242 Using ROIs, the specimens can be segmented and renamed in the rendering software to
243 match the specimen labels (e.g., museum accession number plus straw/capsule position).

244 False-colouring straws or capsule rows differently in the 3D volume also helps to track
245 specimen order. Any specimens with obvious artefacts can be marked with their labels
246 followed by the word 'REDO', to be set aside during unpacking so they can be scanned again
247 under improved conditions, i.e, repositioned in the capsule or with better tissue support.
248

249 **Unpacking and storage**

250 Capsules are unpacked from the straws in the same manner as they were put in, by inserting a
251 cocktail straw into one end and pushing it through (Fig. 2c). We recommend checking
252 specimens off the list as they are being unpacked as a final test of correct labelling. These
253 samples can be stored long-term inside the capsules since archival tissue and paper was used.
254 Specimens for rescanning can be included in the next batch and labelled digitally with their
255 ID, new straw and capsule position, and the word 'REDONE' for transparency. This process
256 can be repeated as many times as necessary to achieve optimal quality scans for all material.
257 Likewise, all labelled straws and Falcon tubes can be reused in subsequent scans, which will
258 further ensure consistency in the packing and labelling process.
259

260 **Results and Discussion**

261 Optimal settings for our fossils in terms of time, resolution and file size were three separate
262 scans of the Falcon tube at 40 mm focus-to-object distance (FOD) and 225 mm focus-to-
263 detector distance (FDD), using 40 kV, 300 µA, and 0.5 s exposure for 1400 images, with a
264 frame average of 3 and image skip of 1. This configuration allowed us to decrease the width
265 of the detector to 2,000 pixels, meaning that each X-ray image was 9.15 MB. The Y-axis of
266 the stage was shifted down by 29 mm between scans to allow some overlap between
267 segments (Fig. 3a). For each segment this resulted in a scan time of 47 minutes and 17.8 µm
268 voxel size, with reconstructed volumes around 10 GB each (Fig. 3b).

269 This process is in stark contrast to the effort needed to scan each specimen
270 individually at the highest resolution (10.6 μm over 5,000 projections for a single size 4
271 capsule), requiring 167 minutes per scan or over eight hours for a fully packed tube,
272 excluding time to swap samples. Automated sample changers are available for some μCT
273 machines (e.g., Bruker SkyScan, Bruker Biosciences Pty Ltd), although these are still limited
274 to under 20 specimens. Reconstructing and rendering each μCT file separately would also
275 require substantial computing time, making the task unfeasible for individual researchers
276 wishing to work on large data sets. Instead, we stitched the three segments together into a
277 volume of equally high resolution (Fig. 3c), allowing access to multiple specimens by
278 opening a single 30 GB file.
279 The image quality achieved by our method was more than adequate for applications in
280 biological systematics, including geometric morphometrics, functional analyses, and
281 morphological descriptions. Cross-sectional μCT images revealed sharp contrast between the
282 hydroxyapatite of the bone, dentine, and enamel against the clay and crystalline calcium
283 carbonate-rich matrix, while offering precise details of specimen morphology as well as the
284 dividing walls of the capsules, straws and paper (Fig. 3d-f). In few cases artefacts were
285 observed in the reconstruction due to movement (Fig. 3g) or beam hardening (Fig. 3h). These
286 specimens were labelled as 'REDO' in the 3D volume and set aside during unpacking to be
287 rescanned, either with additional tissue in the capsule or using a filter, respectively. In earlier
288 scans we observed some capsules in straws that had been slightly crushed by the one above it.
289 These straws were packed using a solid dowel to push down the capsules, hence why we
290 recommend using a cocktail straw instead.
291 Other examples of material scanned using our high-throughput method are shown in
292 Figure 4. Fossilized frog ilia and varanid osteoderms (bony deposits in the scales of some
293 lizards) yielded excellent results following this protocol (Fig. 4ab), with hundreds of 3D

294 models generated for minimal time, money and effort. We also applied our system to larger
295 mammalian specimens, for example fossilized rodent jaws from the Middle Pleistocene Mt
296 Etna[42]. This material is larger and denser than the herpetological samples, requiring slightly
297 different parameters for μCT scanning. For larger/denser fossils, a 0.1 mm copper plate was
298 secured under the collimator to reduce beam hardening and other artefacts, and X-ray voltage
299 was increased to 50-80 kV. The resulting reconstructed images could be easily segmented
300 using density-based approaches in VGStudioMax, like the region growing tool to separate
301 teeth from bone (Fig. 4c).

302 Stewardship of μCT data is still a major challenge for natural history museums, which
303 are now tasked with the curation of rapidly expanding digital datasets associated with the
304 physical collections[43]. There is currently no standard for 3D data storage, meaning that the
305 fate of μCT images and their metadata is often individual or institution-driven. We retain at
306 least two copies of the original X-rays and reconstructions in different locations (one cloud-
307 based, one physical), while working on the prepared volume on a regularly backed-up server.
308 Davies et al.[5] provide a summary of file types that should be retained for 3D digital
309 morphology analyses, with best practices recommended when storage space is not a problem.
310 Online data repositories are another attractive option for long-term data storage, several of
311 which are free and cater to 3D digital datasets generated for biological research[5], e.g., Zenodo
312 (zenodo.org), MorphoSource (www.morphosource.org).

313 For most downstream analyses, μCT data will be converted into polygonal surface
314 models such as STL (sterolithography) files, which capture the geometric shape of a 3D
315 object using triangles or vertices to describe its surface (Fig. 4d). These models, also known
316 as surface meshes, are virtually interactive and can be manipulated, viewed, and measured
317 using the open source software MeshLab (http://meshlab.sourceforge.net/). They are also
318 small in terms of data storage, making them easy to distribute online and providing wider

access to museum collections. Finally, surface meshes can be scaled up for displays and educational programs, for example using 3D printing. Following digital labelling and unpacking of our specimens, we extracted STL models of each fossil from its ROI in VGStudioMax, while retaining its original identity.

Many of the fossils included in this project were excavated from cave deposits at Capricorn Caves in Rockhampton, Queensland, Australia. As part of an annual science communication event called Capricorn Caves Fossil Open Day[44], we 3D printed select specimens to engage the public in local biodiversity. There palaeontologists referred to the enlarged 3D models to assist in the interpretation of microfossils, allowing children to interact with replicas of local animals from thousands of years in the past (Fig. 4e). In addition to public outreach, our future work will focus on analysing the generated µCT data using a growing toolkit of bioinformatic approaches, including machine learning and AI, 3D landmark-based geometric morphometrics, and high-density point cloud comparisons of fossil and living forms (Fig. 4f).

Conclusions

Current research on museum-based µCT data encompasses an extraordinary array of material and topics, including tetrapod origins[45], echolocation in bats[46] and whales[47], limb reduction in lizards[48,49], mammalian limb development[50,51], primate neuroanatomy[52,53], reproduction in insects[54] and plants[55], paleoecology of Precambrian biota[56], seafloor biomass estimation[57] and amber inclusions[58], to name a few. Typically these studies involve few specimens, due to the challenges of capturing high resolution 3D data for large sample sizes.

Here we demonstrate how simple, inexpensive equipment like drinking straws and pharmaceutical capsules can be modified for high-throughput µCT scanning of dozens of fossils in a single container, providing large-scale morphological datasets for comparative

analyses. To date we have scanned over 1,000 accessioned museum specimens following this technique, including hundreds of frogs, lizards, snakes and mammals. These data will contribute to ongoing efforts to identify evolutionary responses to climate change in Australia's fossil record, where reptiles and amphibians constitute half of the terrestrial vertebrate diversity, and where increasing aridity has transformed large parts of the continent. This method can also be adapted for other (non-biological) objects, by creating custom-made holders and stages, and seeking µCT scanners with differing capacities. Some users may wish to scan individual specimens or holotypes at the highest possible resolution, in which case our protocol offers an efficient pathway for determining which specimens should be elevated to type status. At the same time we note that fossils can be difficult to scan, being highly variable in shape, composition, and density. Thus while µCT is a powerful tool for most small specimens, in some cases other non-destructive techniques such as magnetic resonance imaging (MRI), synchrotron, and confocal microscopy may be more appropriate.

Acknowledgements

This work was supported by an Australian Research Council DECRA (DE180100629) to CAH, with scans performed through the Melbourne TrACEES platform. Danielle Measday, Conservator of Natural Sciences at Museums Victoria, advised on and provided archival papers for testing. We thank Kristen Spring, Rochelle Lawrence, Joanne Wilkinson, and Jonathan Cramb, along with many volunteers at the Queensland Museum, for their assistance in generating the large quantity of specimens made available for this project.

Author Contributions

C.A.H. and S.H. conceived the project; S.H. selected specimens for µCT scanning; C.A.H., R.A., and J.R.B. designed the methodology; J.R.B. operated the µCT machine; C.A.H. and

R.A. collected and analysed the data and led manuscript writing. All authors contributed to manuscript drafts and gave final approval for publication.

Competing interests

The authors declare no competing interests.

Data Availability

All X-ray and µCT data shown in Fig. 3a-e are available in the MorphoSource repository, [link provided upon acceptance].

References

1. Sato, T., Ikeda, O., Yamakoshi, Y. & Tsubouchi, M. X-ray tomography for microstructural objects. *Appl. Opt.* **20**, 3880-3883 (1981).

2. Elliott, J. C. & Dover, S. D. X-ray microtomography. *J. Microsc.* **126**, 211-213 (1982).

3. Elliott, J. C. & Dover, S. D. X-ray microscopy using computerized axial tomography. *J. Microsc.* **138**, 329-331 (1985).

4. Sutton, M., Rahman, I. & Garwood, R. Techniques for Virtual Palaeontology. 208 p (Wiley-Blackwell, 2014).

5. Davies, T. G. *et al.* Open data and digital morphology. *Proc. R. Soc. B* **284**, 20170194 (2017).

6. Gutiérrez, Y., Ott, D., Töpperwien, M., Salditt, T. & Scherber, C. X-ray computed tomography and its potential in ecological research: a review of studies and optimization of specimen preparation. *Ecol. Evol.* **8**, 7717-7732 (2018).

7. Schindelin, J. *et al.* Fiji: an open-source platform for biological-image analysis. *Nat. Methods* **9**, 676-682 (2012).

8. Ketcham, R. A. Computational methods for quantitative analysis of three-dimensional features in geological specimens. *Geosphere* **1**, 32-41 (2005).

9. Page, L. M., MacFadden, B. J., Fortes, J. A., Soltis, P. S. & Riccardi, G. Digitization of biodiversity collections reveals biggest data on biodiversity. *BioScience* **65**, 841-842 (2015).

10. Faulwetter, S., Vasileiadou, A., Kouratoras, M., Dailianis, T. & Arvanitidis, C. Micro-computed tomography: Introducing new dimensions to taxonomy. *ZooKeys* **263**, 1-45 (2013).

11. Akkari, N. *et al*. New avatars for Myriapods: complete 3D morphology of type specimens transcends conventional species description (Myriapoda, Chilopoda). *PLoS ONE* **13**, 0200158; 10.1371/journal.pone.0200158 (2018).

12. Fontaine, B., Perrard, A. & Bouchet, P. 21 years of shelf life between discovery and description of new species. *Curr. Biol*. **22**, R943-R944 (2012).

13. Hipsley, C. A. & Sherratt, E. Psychology, not technology, is our biggest challenge to open digital morphology data. *Sci. Data*. **6**, 41 (2019).

14. Blagoderov, V., Kitching, I. J., Livermore, L., Simonsen, T. J. & Smith, V. S. No specimen left behind: industrial scale digitization of natural history collections. *Zookeys* **209**, 133-146 (2012).

15. Rogers, N. Museum drawers go digital. *Science* **352**, 762-765 (2016).

16. Meineke, E. K., Davies, T. J., Daru, B. H. & Davis, C. C. Biological collections for understanding biodiversity in the Anthropocene. *Phil. Trans. R. Soc. B* **374**, 20170386 (2018).

17. Schmitt, C. J., Cook, J. A., Zamudio, K. R. & Edwards, S.V. Museum specimens of terrestrial vertebrates are sensitive indicators of environmental change in the Anthropocene. *Phil. Trans. R. Soc. B* **374**, 20170387 (2018)

419

420 18. Sherratt, E., Gower, D. J., Klingenberg, C. P. & Wilkinson, M. Evolution of cranial shape
421 in caecilians (Amphibia: Gymnophiona). *Evol. Biol.* **41**, 528-545 (2014).
422 19. Watanabe, A. *et al.* Ecomorphological diversification in squamates from conserved
423 pattern of cranial integration. *Proc. Natl. Acad. Sci*. **116**, 14688-14697 (2019).
424 20. Simon, M. N., Machado, F. A. & Marroig, G. High evolutionary constraints limited
425 adaptive responses to past climate changes in toad skulls. *P. Roy. Soc. B-Biol. Sci.* **283**,
426 20161783 (2016).
427 21. Sherratt, E., Serb, J. M. & Adams, D. C. Rates of morphological evolution, asymmetry
428 and morphological integration of shell shape in scallops. *BMC Evol. Biol.* **17**, 248 (2017).
429 22. Chira, A. M. *et al.* Correlates of rate heterogeneity in avian ecomorphological traits. *Ecol.*
430 *Lett*. **21**, 1505-1514 (2018).
431 23. Percival, C. J. *et al.* The effect of automated landmark identification on morphometric
432 analyses. *J. Anat.* **234**, 917-935 (2019).
433 24. Bouxsein, M. L. *et al.* Guidelines for assessment of bone microstructure in rodents using
434 micro –computed tomography. *J. Bone Miner. Res.* **25**, 1468-1486 (2010).
435 25. Broeckhoven, C. & du Plessis, A. X-ray microtomography in herpetological research: a
436 review. *Amphibia-Reptilia* **39**, 377-401 (2018).
437 26. Marcy, A. E., Fruciano, C., Phillips, M. J., Mardon, K. & Weisbecker, V. Low resolution
438 scans can provide a sufficiently accurate, cost- and time-effective alternative to high
439 resolution scans for 3D shape analyses. *PeerJ* **6**, 5032; 10.7717/peerj.5032 (2018).
440 27. Gray, J. A., McDowell, M. C., Hutchinson, M. N. & Jones, M. E. Geometric
441 morphometrics provides an alternative approach for interpreting the affinity of fossil lizard
442 jaws. *J. Herpetol*. **51**, 375-382 (2017).

443 28. Thorn, K. M., Hutchinson, M. N., Archer, M. & Lee, M. S. Y. A new scincid lizard from
444 the Miocene of northern Australia, and the evolutionary history of social skinks (Scincidae:
445 Egerniinae). *J. Vertebr. Paleontol*. **39**, 1 (2019).
446 29. Chaplin, K., Sumner, J., Hipsley, C. A. & Melville, J. An integrative approach using
447 phylogenomics and high-resolution x-ray computed tomography for species delimitation in
448 cryptic taxa. *Syst. Biol.* **69**, syz048; 10.1093/sysbio/syz048 (2019).
449 30. Melville, J. *et al.* Integrating phylogeography and high-resolution x-ray CT reveals five
450 new cryptic species and multiple hybrid zones among Australian earless dragons. *R. Soc.*
451 *Open Sci.* **6**, 191166; 10.1098/rsos.191166 (2019).
452 31. Caro, A., Gómez-Moliner, B. J. & Madeira, M. J. Integrating multilocus DNA data and
453 3D geometric morphometrics to elucidate species boundaries in the case of *Pyrenaearia*
454 (Pulmonata: Hygromiidae). *Mol. Phylogenet. Evol.* **132**, 194-206 (2019).
455 32. Winkelmann, C. T. & Wise, L. D. High-throughput micro-computed tomography imaging
456 as a method to evaluate rat and rabbit fetal skeletal abnormalities for developmental toxicity
457 studies. J. Pharmacol. Tox. Met. **59**, 156-165 (2009).
458 33. Sevilla, R. S. *et al.* Development and optimization of a high-throughput micro-computed
459 tomography imaging method incorporating a novel analysis technique to evaluate bone
460 mineral density of arthritic joints in a rodent model of collagen induced arthritis. *Bone* **73**, 32-
461 41 (2015).
462 34. Wong, M. D., Maezawa, Y., Lerch, J. P. & Henkelman, R. M. Automated pipeline for
463 anatomical phenotyping of mouse embryos using micro-CT. *Development* **141**, 2533-2541
464 (2014).
465 35. Wu, D. *et al.* Combining high-throughput micro-CT-RGB phenotyping and genome-wide
466 association study to dissect the genetic architecture of tiller growth in rice. *J. Exp. Bot.* **70**,
467 545-561 (2019).

36. Ding, Y. *et al.* Computational 3D histological phenotyping of whole zebrafish by X-ray histotomography. *Elife* **8**, 44898; 10.7554/eLife.44898.001 (2019).

37. Staedtler, Y. M., Masson, D. & Schönenberger, J. Plant tissues in 3D via X-ray tomography: simple contrasting methods allow high resolution imaging. *PLoS ONE* **8**, 75295; 10.1371/journal.pone.0075295 (2013).

38. Keklikoglou, K. *et al.* Micro-computed tomography for natural history specimens: a handbook of best practice protocols. *Eur. J. Taxon*. **522**, 1-55 (2019).

39. Adams, D., Collyer, M. & Kaliontzopoulou, A. Geomorph: Software for geometric morphometric analyses. R package version 3.1.0. https://cran.r-project.org/package=geomorph (2019).

40. Klingenberg, C. P. MorphoJ: an integrated software package for geometric morphometrics. *Mol. Ecol. Resour*. **11**, 353-357 (2011).

41. du Plessis, A., Broeckhoven, C., Guelpa, A. & le Roux, S. G. Laboratory x-ray micro-computed tomography: a user guideline for biological samples. *Gigascience* **6**, 1-11 (2017).

42. Hocknull, S. A., Zhao, J. X., Feng, Y. X. & Webb, G. E. Responses of middle Pleistocene rainforest vertebrates to climate change in Australia. *Earth Planet. Sc. Lett.* **264**, 317-331 (2007).

43. Hedrick, B. P. *et al.* Digitization and the future of natural history collections. *BioScience* **70**, 243-251 (2020).

44. Lawrence, R. A. & Hocknull, S. Engaging the public with small vertebrate fossils and utilizing citizen science to maximise scientific discovery at Capricorn Caves, Central Eastern Queensland, Australia. *J. Vertebr. Paleontol. Program and Abstracts* **139** (2019).

45. Long, J. A., Young, G. C., Holland, T., Senden, T. J. & Fitzgerald, E. M. An exceptional Devonian fish from Australia sheds light on tetrapod origins. *Nature* **444**, 199-202 (2006).

492 46. Arbour, J. H., Curtis, A. A. & Santana, S. E. Signatures of echolocation and dietary
493 ecology in the adaptive evolution of skull shape in bats. *Nat. Commun.* **10**, 2036 (2019).
494 47. Park, T., Fitzgerald, E. M. & Evans, A. R. Ultrasonic hearing and echolocation in the
495 earliest toothed whales. *Biol. Lett.* **12**, 20160060; 10.1098/rsbl.2016.0060 (2016).
496 48. Müller, J. *et al.* Eocene lizard from Germany reveals amphisbaenian origins. *Nature* **473**,
497 364-367 (2011).
498 49. Miralles, A. *et al.* Distinct patterns of desynchronized limb regression in Malagasy
499 scincine lizards (Squamata, Scincidae). *PLoS ONE* **10**, 0126074;
500 10.1371/journal.pone.0126074 (2015).
501 50. Weisbecker, V. Monotreme ossification sequences and the riddle of mammalian skeletal
502 development. *Evolution* **65**, 1323-1335 (2011).
503 51. Newton, A. H. *et al.* Letting the 'cat' out of the bag: pouch young development of the
504 extinct Tasmanian tiger revealed by X-ray computed tomography. *R. Soc. Open Sci.* **5**,
505 171914; 10.1098/rsos.171914 (2018).
506 52. Hublin, J. J. *et al.* New fossils from Jebel Irhoud, Morocco and the pan-African origin of
507 Homo sapiens. *Nature* **546**, 289-292 (2017).
508 53. Beaudet, A. & Gilissen, E. Fossil primate endocasts: perspectives from advanced imaging
509 techniques in *Digital Endocasts: from Skulls to Brains* (eds. Bruner, E., Ogihara, N. &
510 Tanabe, H.) 47-58 (Springer, 2018).
511 54. Wulff, N. C., Lehmann, A. W., Hipsley, C. A. & Lehmann, G. U. C. Copulatory courtship
512 by bushcricket genital titillators revealed by functional morphology, µCT scanning for 3D
513 reconstruction and female sense structures. *Arthropod Struct. Dev.* **44**, 388-397 (2015).
514 55. Gee, C. T. Applying microCT and 3D visualization to Jurassic silicified conifer seed
515 cones: a virtual advantage over thin-sectioning. *Appl. Plant Sci.* **1**, 1300039;
516 10.3732/apps.1300039 (2013).

517 56. Meyer, M. *et al.* Three-dimensional microCT analysis of the Ediacara fossil *Pteridinium*
518 simplex sheds new light on its ecology and phylogenetic affinity. *Precambrian Res.* **249**, 79-
519 87 (2014).
520 57. Gooday, A. J., Sykes, D., Goral, T., Zubkov, M. V. & Glover, A.G. Micro-CT 3D
521 imaging reveals the internal structure of three abyssal xenophyophore species (Protista,
522 Foraminifera) from the eastern equatorial Pacific Ocean. *Sci. Rep.* **8**, 12103; 10.1038/s41598-
523 018-30186-2 (2018).
524 58. Dunlop, J. A. *et al.* Microtomography of the Baltic amber tick *Ixodes succineus* reveals
525 affinities with the modern Asian disease vector *Ixodes ovatus*. *BMC Evol. Biol.* **16**, 203
526 (2016).
527

528

Figures

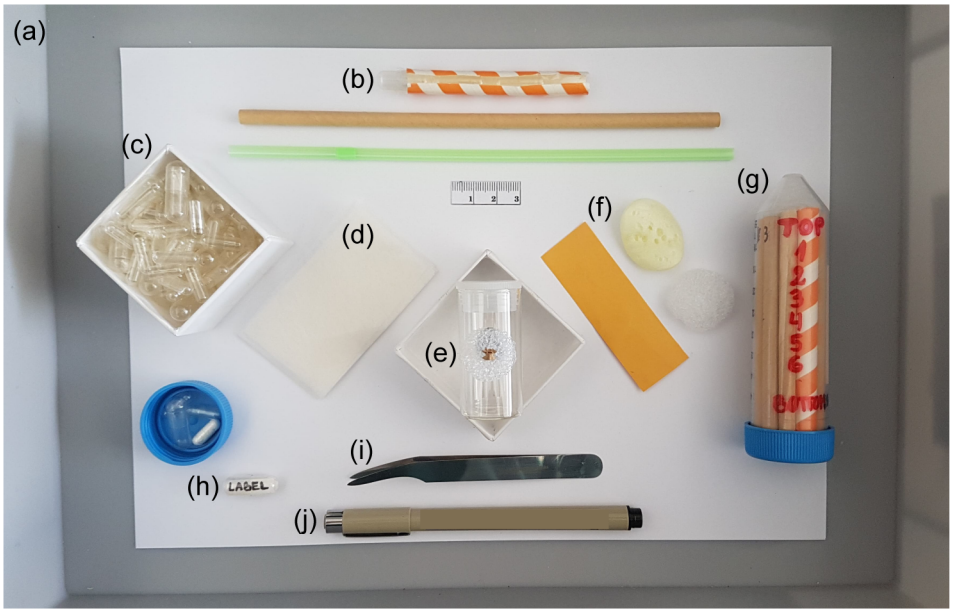

Figure 1. Equipment for dense fossil packing prior to µCT scanning: (a) litter tray, (b) paper and/or plastic straws, (c) clear two-piece pharmaceutical capsules, (d) archival tissue, (e) dry fossil specimen, (f) supporting material (paper, foam), (g) centrifuge tube with cap, (h) archival paper for labels shown inside a size 4 capsule, (i) forceps, (j) archival pen. Estimated costs and material suppliers are listed in Table 1.

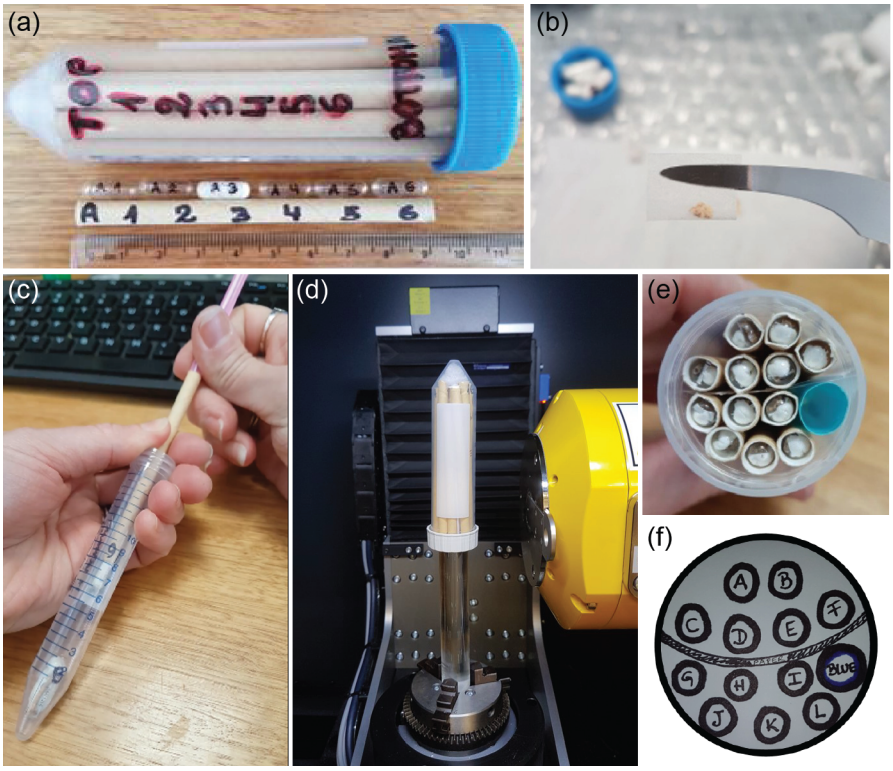

Figure 2. Specimen labelling and packing: (a) 50 ml Falcon tube with a labelled straw and capsules, (b) a single fossil wrapped in Green's Lens tissue to minimise movement during image acquisition, (c) loading capsules into the paper straw using a thinner cocktail straw to gently push them down, (d) a packed 50 ml Falcon tube mounted on a glass rod inside the µCT machine; note that the cap-side is facing down (e) the packed tube from above, and (f) the diagram of straw arrangements in (e), noting the position of a larger blue straw and paper used as a divider.

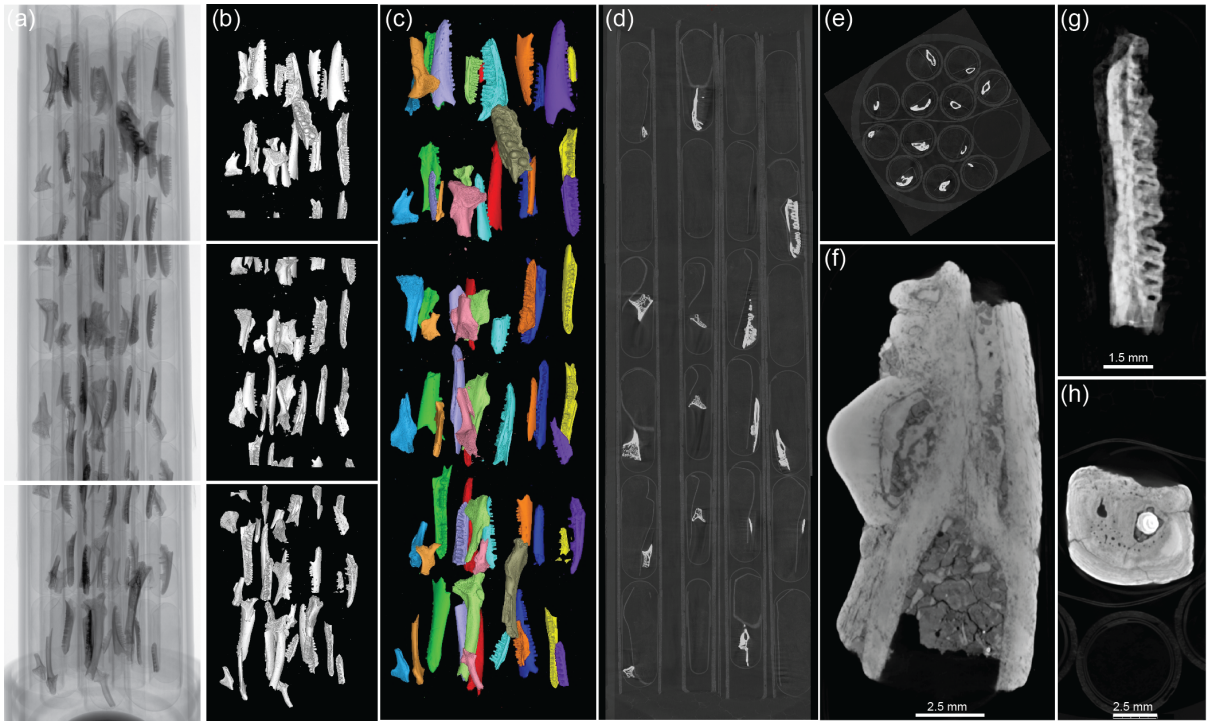

Figure 3. High-throughput µCT results: (a) the first X-ray image from each scanned segment of the 50 ml tube from top (tip) to bottom (cap), containing 72 frog and lizard specimens. (b) 3D renderings of the individual segments in the same positions, at 17.8 µm voxel size, (c) the stitched 3D volume at the same resolution, with fossils colour-coded by straw, (d) reconstructed cross-section of the same tube in side and (e) top views, (f) cross-section of an agamid lizard jaw showing contrast between the matrix, bone, and teeth, (g) cross-section of a skink mandible with a shadow motion artefact, (h) an example of beam hardening caused by a dense surface.

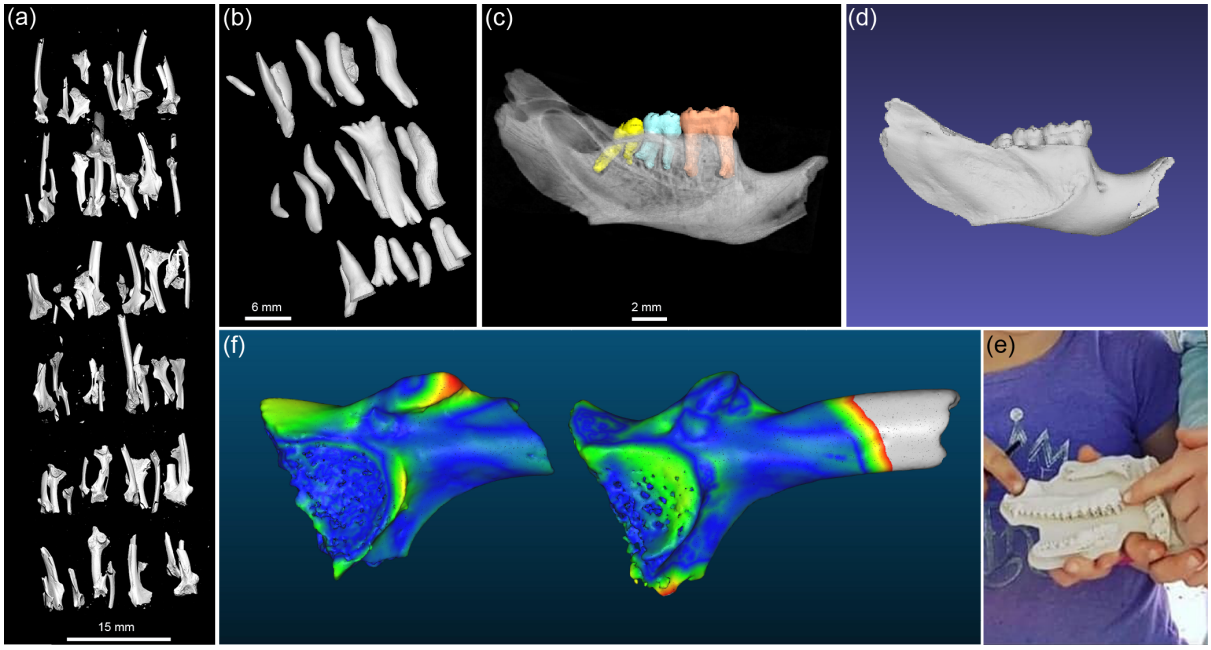

Figure 4. Scanned fossil material and its applications: (a) 3D rendering of 73 fossil frog ilia scanned in a single tube, (b) a subsample of varanid osteoderms in 3D, (c) mandible of the rainforest rodent *Pogonomys* from the Riversleigh World Heritage site with molars colour coded and jaw bone rendered semi-transparent, (d) surface mesh of the same specimen composed of 109,213 vertices (file size 10.5 MB), (e) photograph of children holding a 3D print of enlarged fossil skink jaws at Capricorn Caves Fossil Open Day, (f) point cloud comparison of fossil tree frog (Hylidae) ilia found in Capricorn Caves at 10-20 cm depth (left) and 40-50 cm depth (right), representing a time difference of 2-3,000 years. Warmer colours denote regions with greater shape differences, as estimated in CloudCompare v.2.10.2.

571 **Tables**

572

573 Table 1. Estimated costs in Australian dollars (AUD) for material to µCT scan a 50 ml
574 cylinder fully packed with 84 capsules holding 1 small (< 1 cm long) specimen each. Note
575 that many items (e.g., Falcon tube, straws, forceps, foam, litter tray, pen) can be reused
576 multiple times, thus decreasing the cost for subsequent scans.

577

Item	Total cost per scan (AUD)
Centrifuge Falcon Tube 50 mL polypropylene (PP), conical bottom with screw cap[1]	0.60
Hard 2-piece clear gelatine capsules, size 4 (volume 0.23 ml)[2*]	2.10
Standard paper straw (6 x 135 mm)[3]	0.27
Green's Lens Tissue, un-buffered TIS-L Soft, acid-free, long fibred 9gsm repair/wrapping tissue (609 x 914 mm)[4]	0.76
Feather Forcep Sharp E122S, 0.23 mm gauge thick[5]	4.90
Ethafoam 220, medium density, non-cross linked Polyethylene (PE) closed cell foam (2400 x1200 mm)[6]	1.00
Litter tray[7]	4.00
Label paper[8]	0.10
Archival pen [9]	6.54
TOTAL	20.30

578 Suppliers: [1]https://corning.com.au; [2]https://gelcapsules.com.au; [3]https://www.greenpack.com.au;
579 [4]http://www.archivalsurvival.com.au; [5]http://www.entosupplies.com.au;
580 [6]https://www.foamsales.com.au; [7]https://www.kmart.com.au; [8]https://www.talasonline.com;
581 [9]https://www.newtownartsupplies.com.au/
582 *Clear 2-piece vegetable capsules are also available, although we did not test their performance in
583 µCT scans.
584

585

586 Table 2. Estimated movement among 408 fossils µCT scanned using various packing

587 materials to secure the specimen inside each capsule.

588

Packing material	Number of specimens per capsule (size 4) that moved during scanning			Archival?	Comments
	1-2	3	> 3		
Green's Lens[1]	0/100 (0%)	2/39 (5.1%)	25/50 (50%)	Yes	Ideal consistency
Kim Tech wipes[2]	0/100 (0%)	4/39 (10.3%)	27/50 (54%)	No	100% fibre, not acid free
Ethafoam 220[3]	10/10 (100%)	10/10 (100%)	10/10 (100%)	No	Slippery and hard
Tyvek[4]	-	-	-	Yes	Not tested, too waxy
Renaissance[5]	-	-	-	Yes	Not tested, too rigid

589 Suppliers: [1]http://www.archivalsurvival.com.au; [2]https://www.kcprofessional.com.au;
590 [3]https://www.foamsales.com.au; [4]http://www.dupont.com.au; [5]http://www.lightimpressionsdirect.com